Supporting Information

Heteroleptic Cationic Iridium(III) Complexes Bearing Naphthalimidyl Substituents: Synthesis, Photophysics and Reverse Saturable Absorption

Chengkui Pei,[a] Peng Cui,[a,b] Christopher McCleese,[c] Svetlana Kilina,[a,*] Clemens Burda,[c,*] Wenfang Sun[a,*]

[a]*Department of Chemistry and Biochemistry, North Dakota State University, Fargo, North Dakota 58108-6050, United States*

[b]*Materials and Nanotechnology Program, North Dakota State University, North Dakota 58108, United States*

[c]*Department of Chemistry, Case Western Reserve University, Cleveland, Ohio 44106, United States*

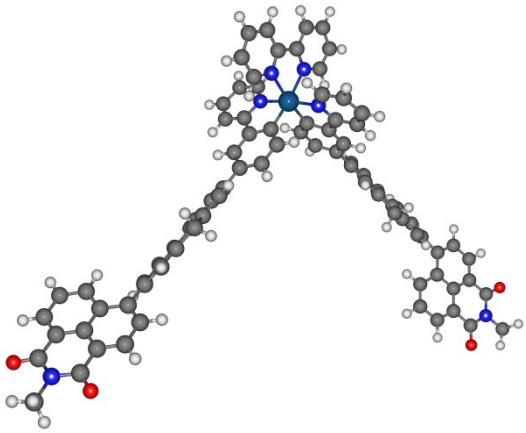

Ir-1

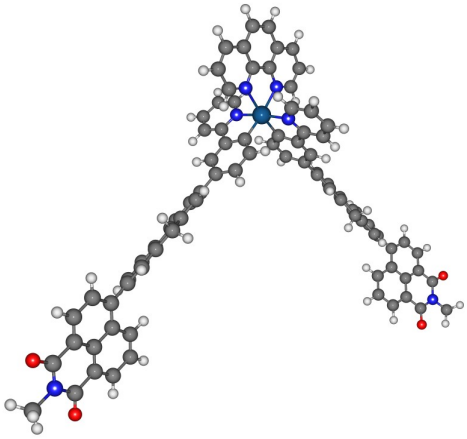

Ir-2

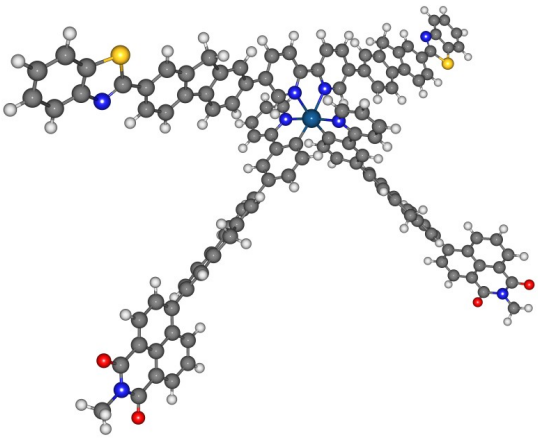

Ir-3

Figure S1. Optimized ground-state geometry of **Ir-1 – Ir-3** in CH_2Cl_2 at the DFT level of theory.

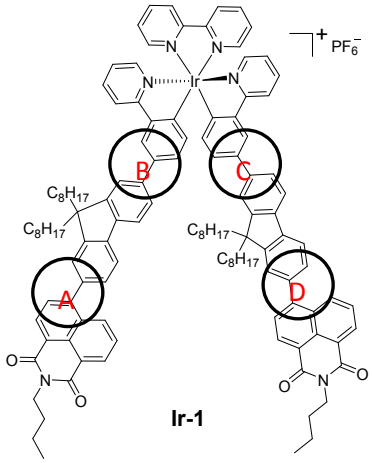

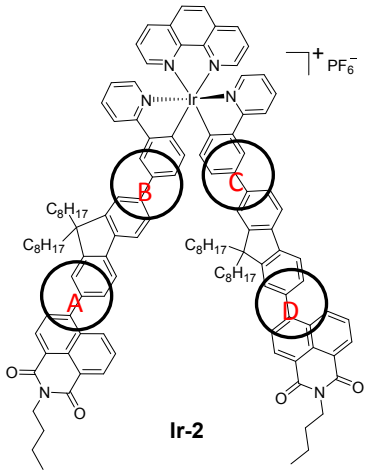

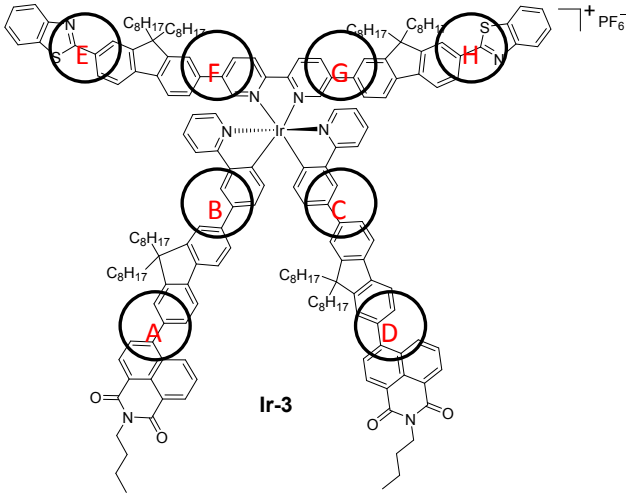

Table S1. Dihedral angles between different parts in the C^N ligand for **Ir-1 – Ir-3**

Complex	Dihedral angle (°)							
	A	B	C	D	E	F	G	H
Ir-1	52.82	37.53	36.69	53.06	-	-	-	-
Ir-2	50.26	36.01	35.38	52.97	-	-	-	-
Ir-3	49.80	35.78	35.61	53.16	0.65	34.40	33.80	0.92

Ir-1

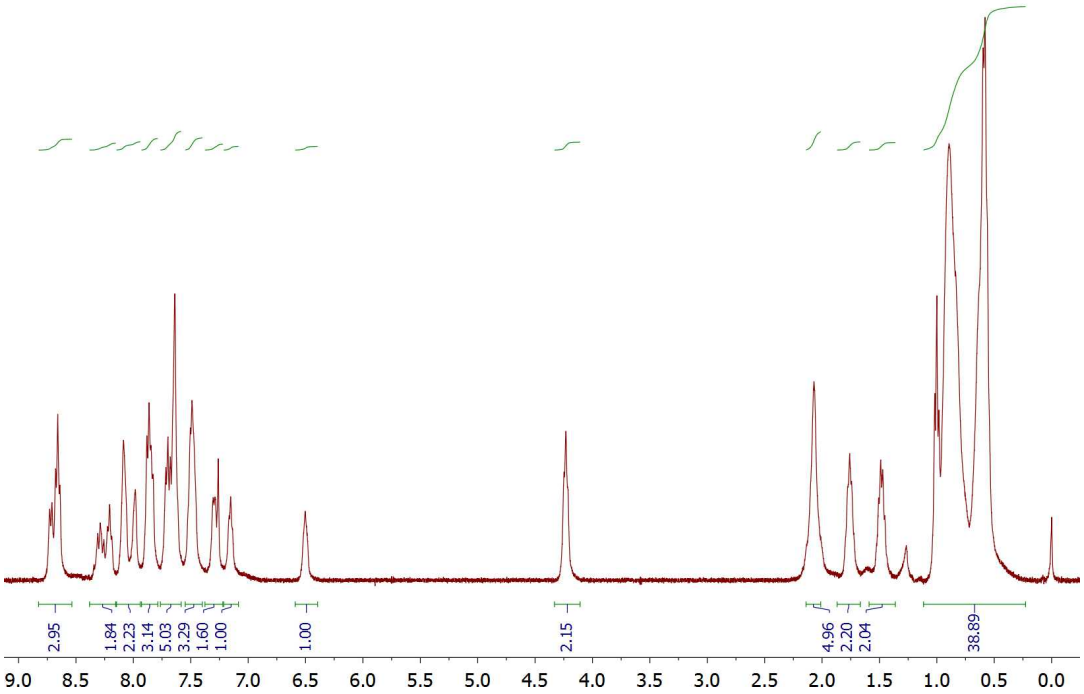
2.95
1.84
2.23
3.14
5.03
3.29
1.60
1.00
1.00
2.15
4.96
2.20
2.04
38.89
9.0 8.5 8.0 7.5 7.0 6.5 6.0 5.5 5.0 4.5 4.0 3.5 3.0 2.5 2.0 1.5 1.0 0.5 0.0

Ir-2

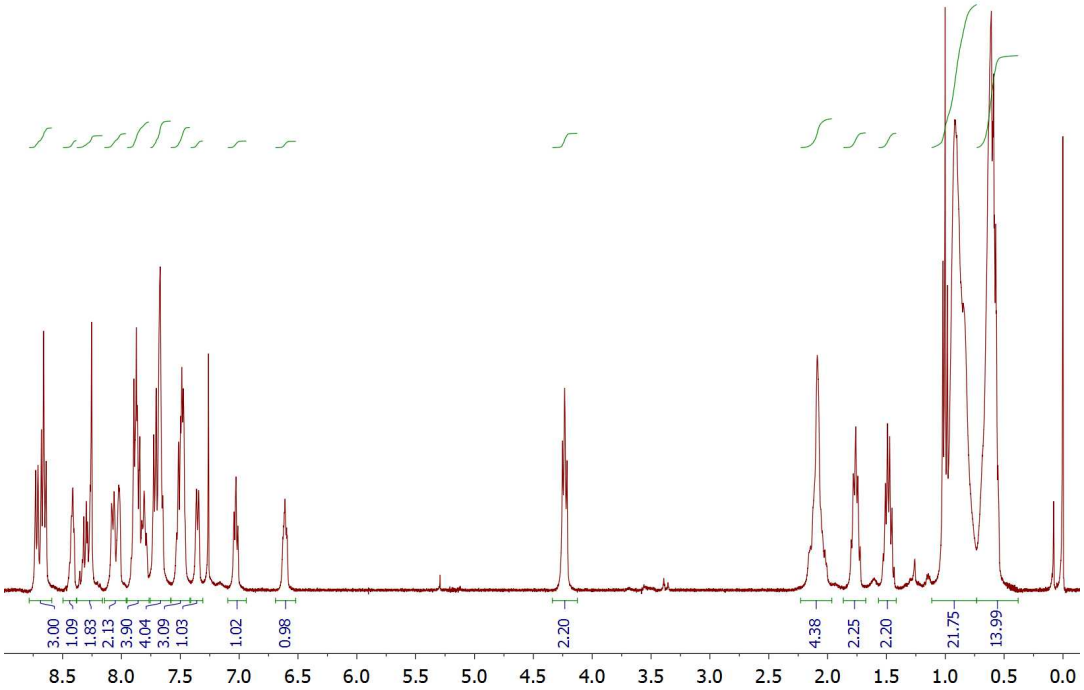
3.00
1.09
1.83
2.13
3.90
4.04
3.09
1.03
1.02
0.98
2.20
4.38
2.25
2.20
21.75
13.99
8.5 8.0 7.5 7.0 6.5 6.0 5.5 5.0 4.5 4.0 3.5 3.0 2.5 2.0 1.5 1.0 0.5 0.0

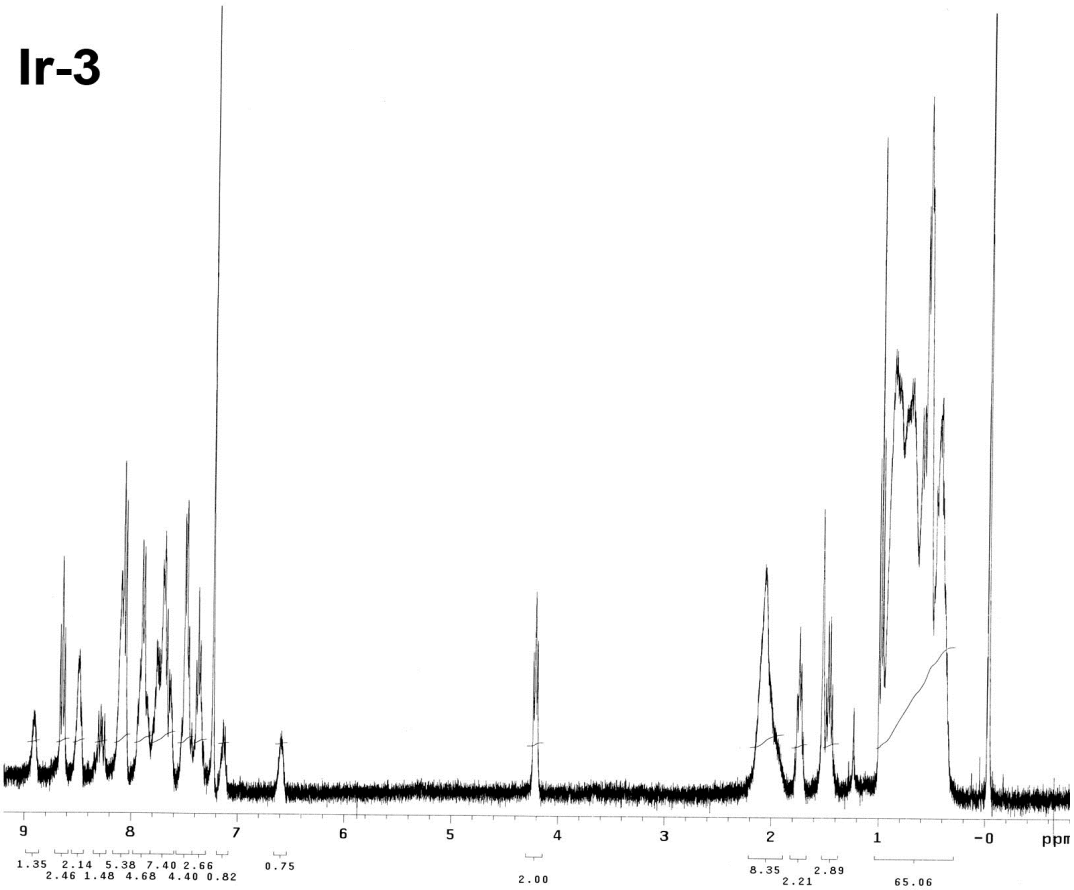

Figure S2. ^{1}H-NMR spectra of **Ir-1 – Ir-3** in $CDCl_3$ at r.t.

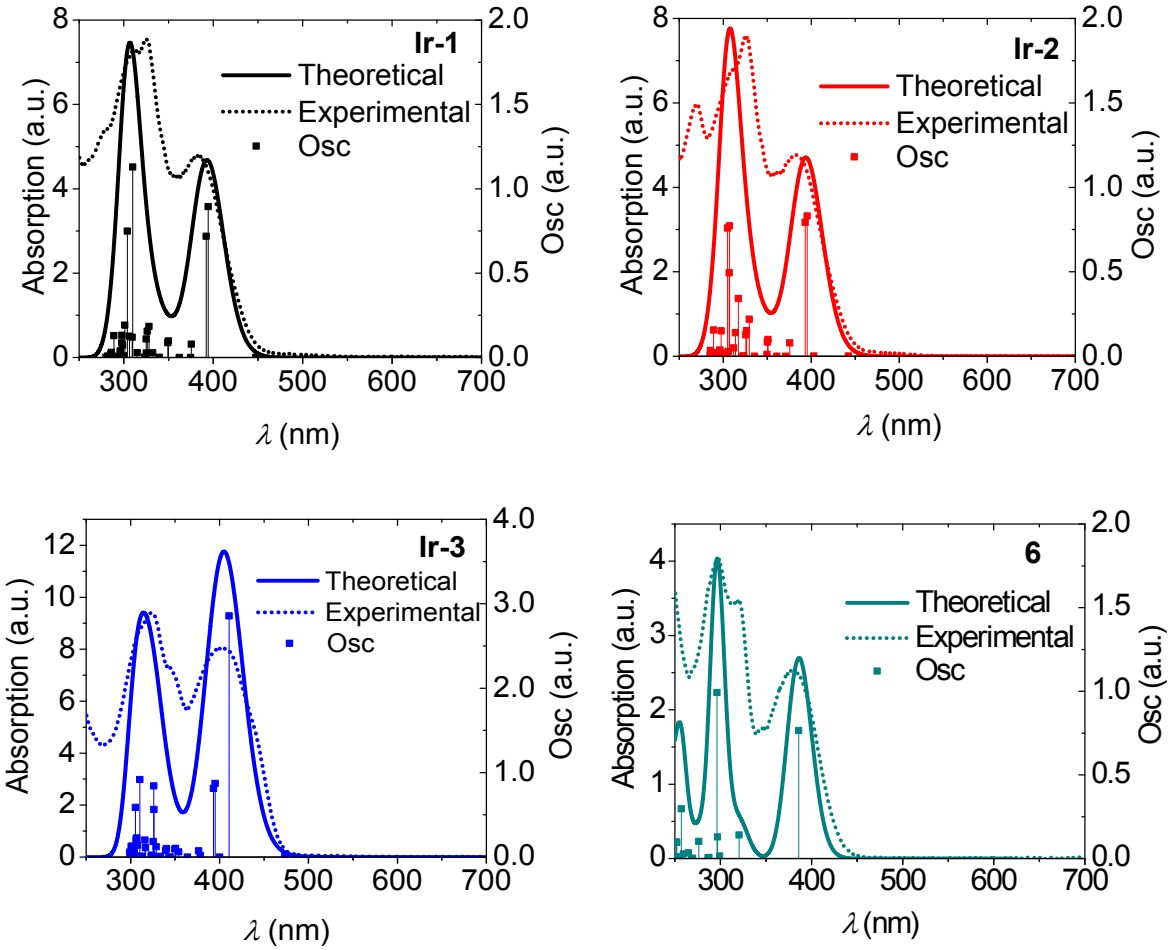

Figure S3. Comparison of the experimental and calculated UV-vis absorption spectra of **Ir-1 – Ir-3** and ligand **6** in CH_2Cl_2.

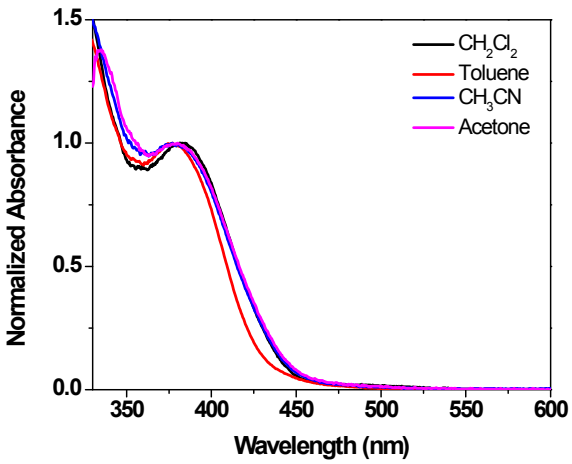

Figure S4. Normalized UV-vis absorption spectra of **Ir-1** in different solvents.

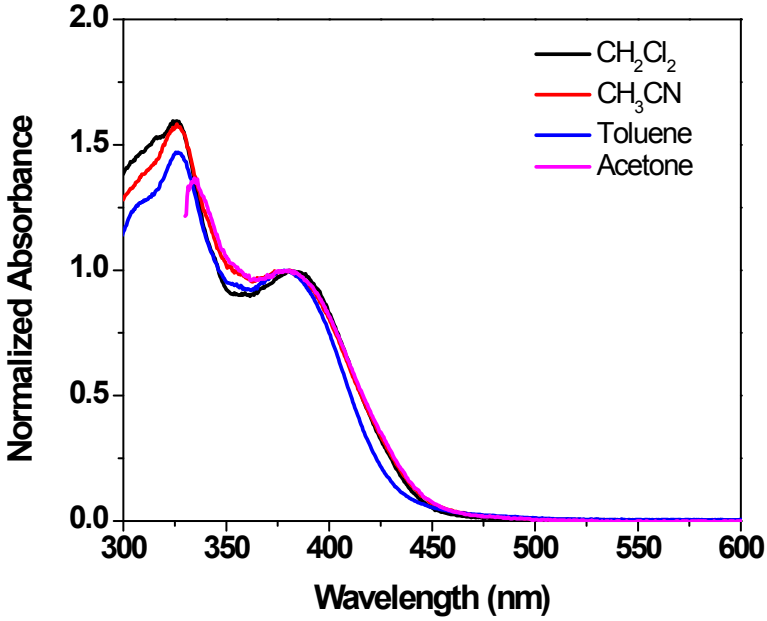

Figure S5. Normalized UV-vis absorption spectra of **Ir-2** in different solvents.

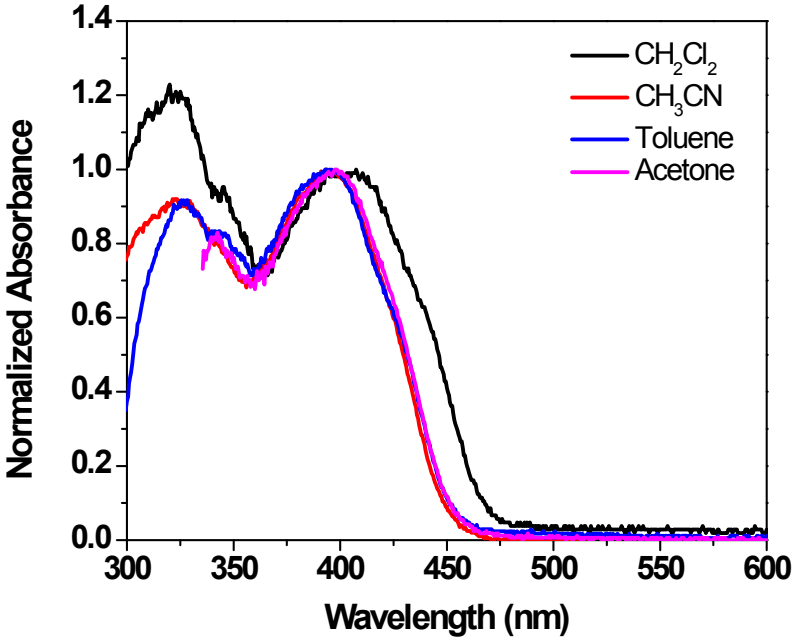

Figure S6. Normalized UV-vis absorption spectra of **Ir-3** in different solvents.

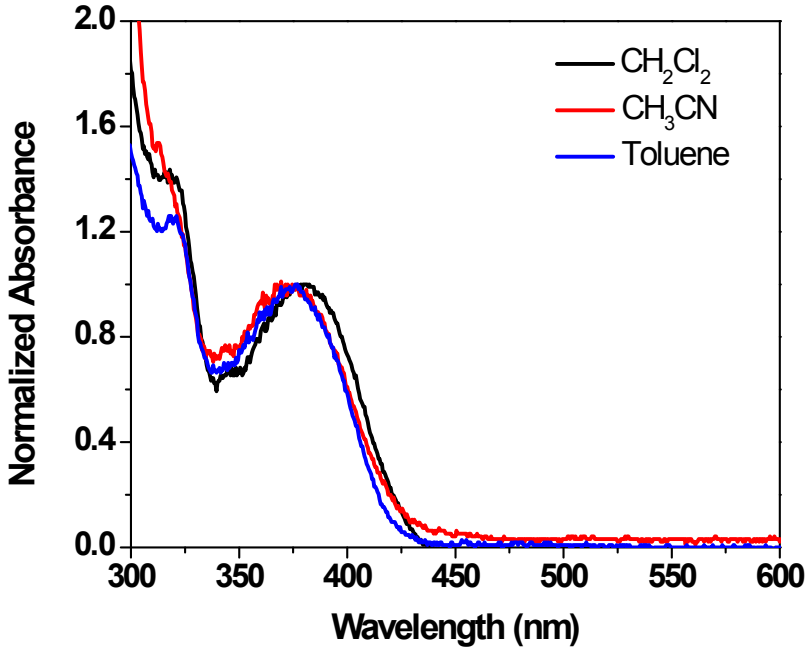

Figure S7. Normalized UV-vis absorption spectra of ligand **6** in different solvents.

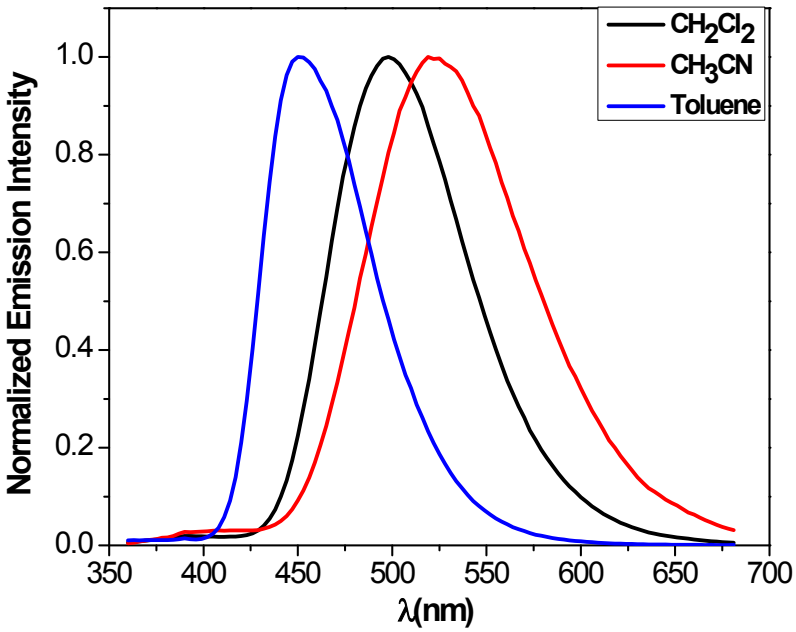

Figure S8. Normalized emission spectra of ligand **6** in different solvents (excited at 347.5 nm).

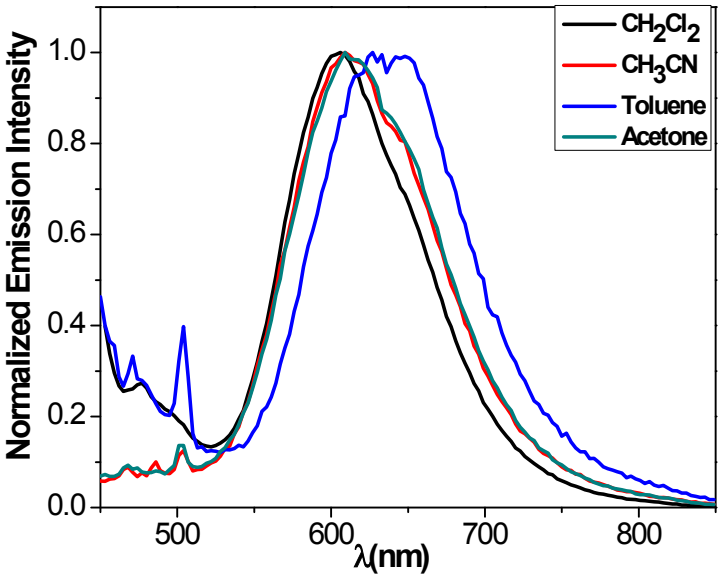

Figure S9. Normalized emission spectra of **Ir-1** in different solvents (excited at 436 nm).

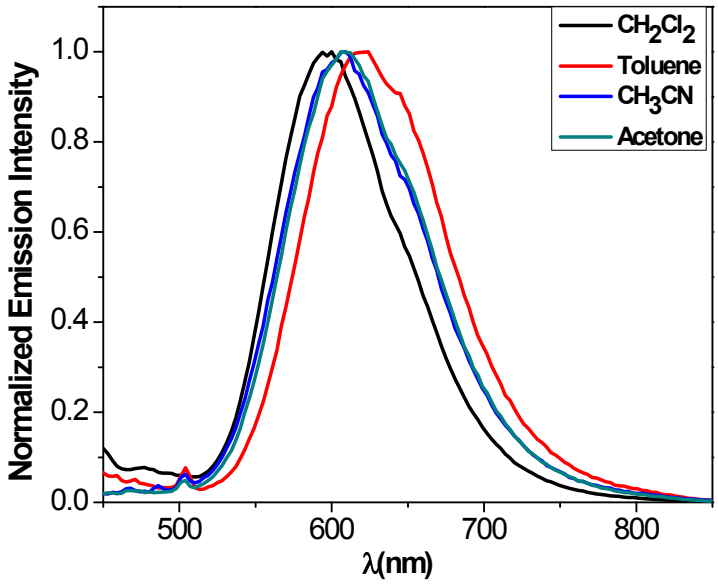

Figure S10. Normalized emission spectra of **Ir-2** in different solvents (excited at 436 nm).

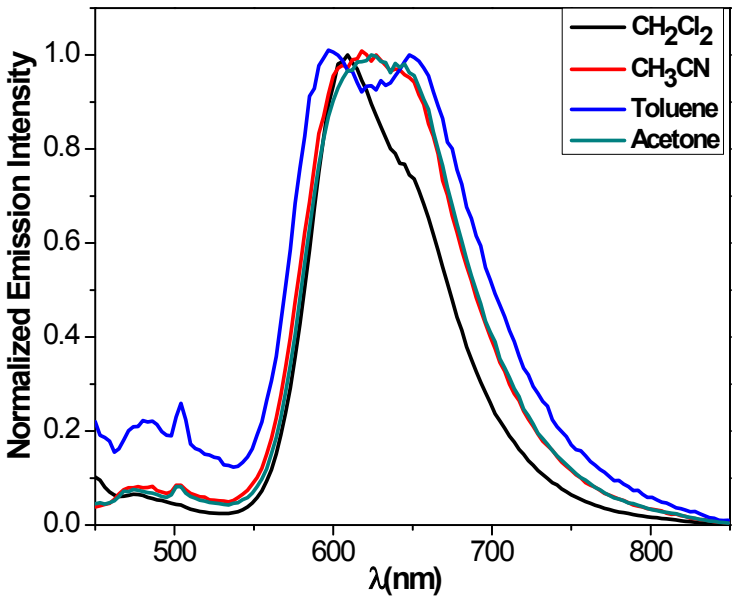

Figure S11. Normalized emission spectra of **Ir-3** in different solvents (excited at 436 nm).

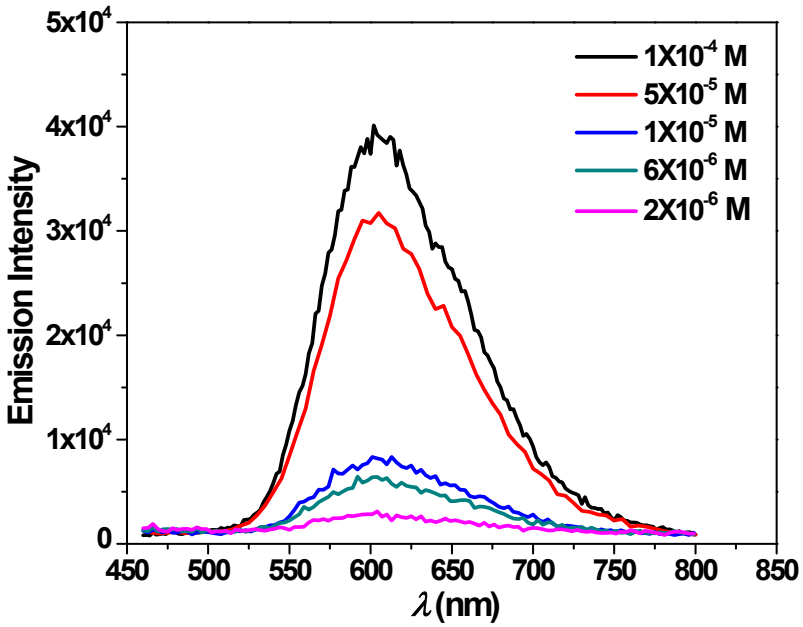

Figure S12. Emission spectra of **Ir-1** at different concentrations excited at 450 nm.

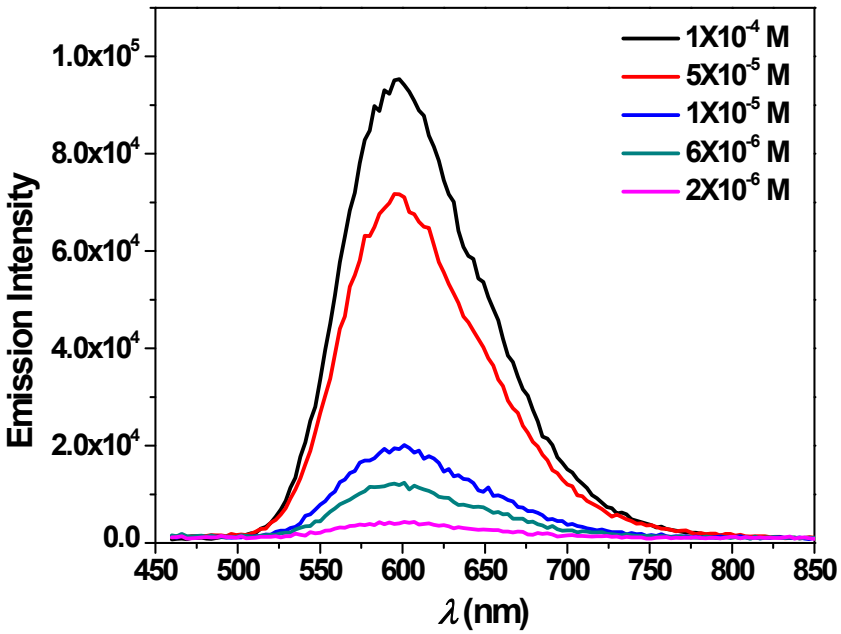

Figure S13. Emission spectra of **Ir-2** at different concentrations excited at 450 nm.

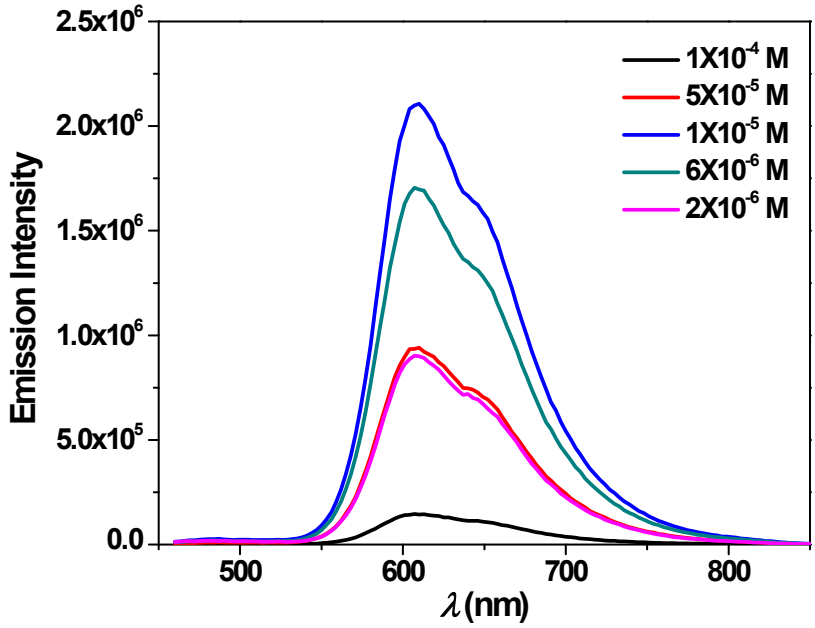

Figure S14. Emission spectra of **Ir-3** at different concentrations excited at 450 nm.

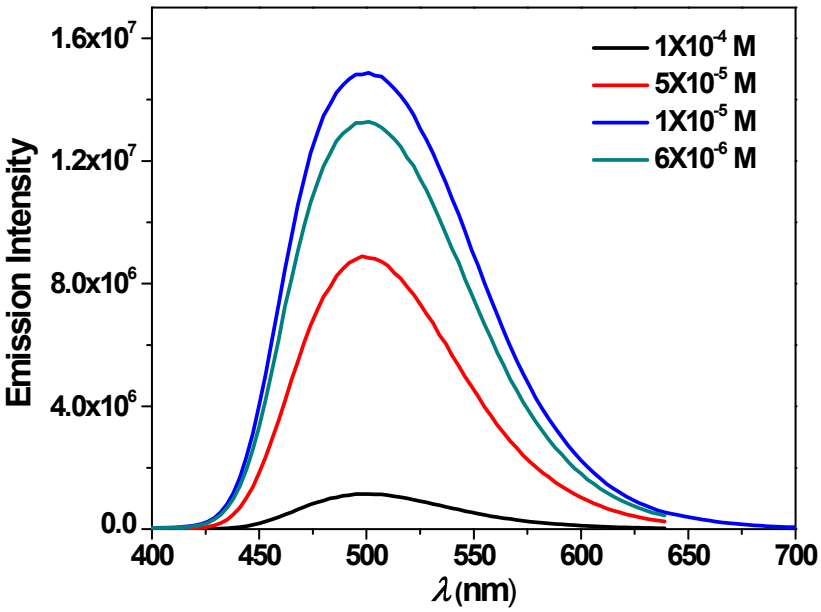

Figure S15. Emission spectra of ligand **6** at different concentrations excited at 379 nm.

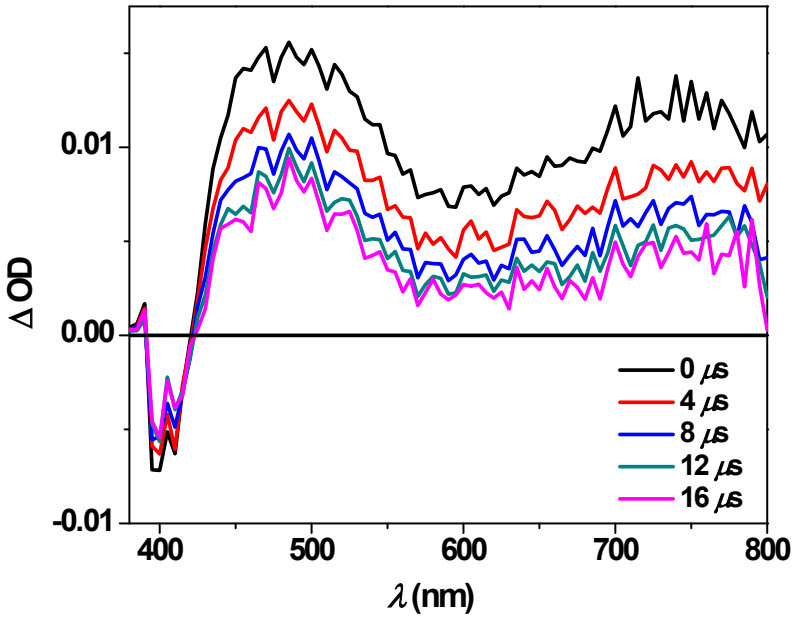

Figure S16. Nanosecond time-resolved transient differential absorption spectra of **Ir-1** in CH_2Cl_2. λ_{ex} = 355 nm, $A_{355\ nm}$ = 0.4 in a 1-cm cuvette.

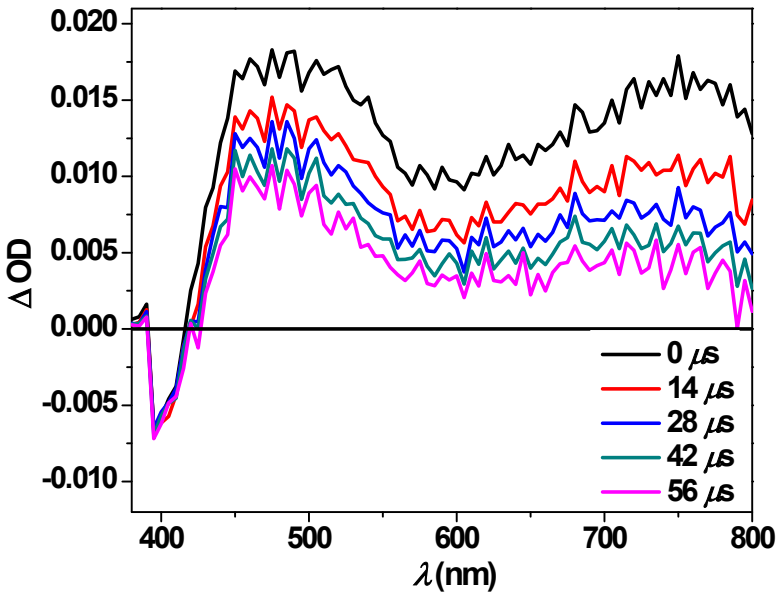

Figure S17. Nanosecond time-resolved transient differential absorption spectra of **Ir-2** in CH_2Cl_2. λ_{ex} = 355 nm, $A_{355\ nm}$ = 0.4 in a 1-cm cuvette.

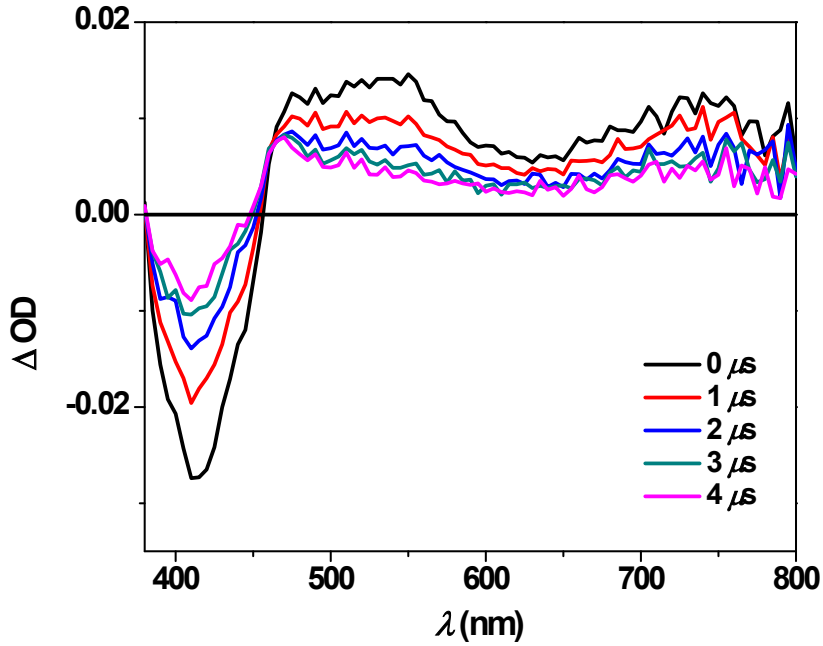

Figure S18. Nanosecond time-resolved transient differential absorption spectra of **Ir-3** in CH_2Cl_2. λ_{ex} = 355 nm, $A_{355\ nm}$ = 0.4 in a 1-cm cuvette.

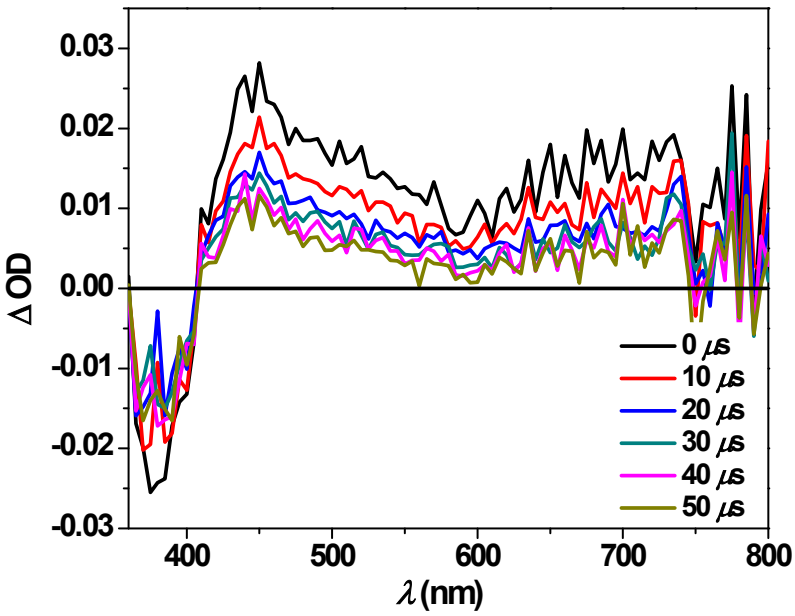

Figure S19. Nanosecond time-resolved transient differential absorption spectra of ligand **6** in CH_2Cl_2. λ_{ex} = 355 nm, $A_{355\ nm}$ = 0.4 in a 1-cm cuvette.

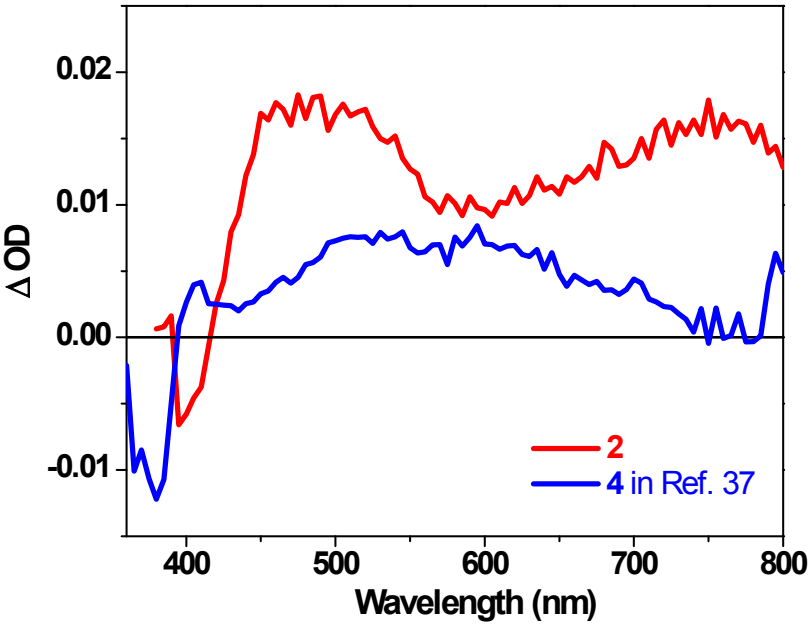

Figure S20. Comparison of the nanosecond transient differential absorption spectra of **Ir-2** in CH_2Cl_2 and complex **4** in Ref. 37 in toluene at zero delay after excitation. λ_{ex} = 355 nm, $A_{355\ nm}$ = 0.4 in a 1-cm cuvette.

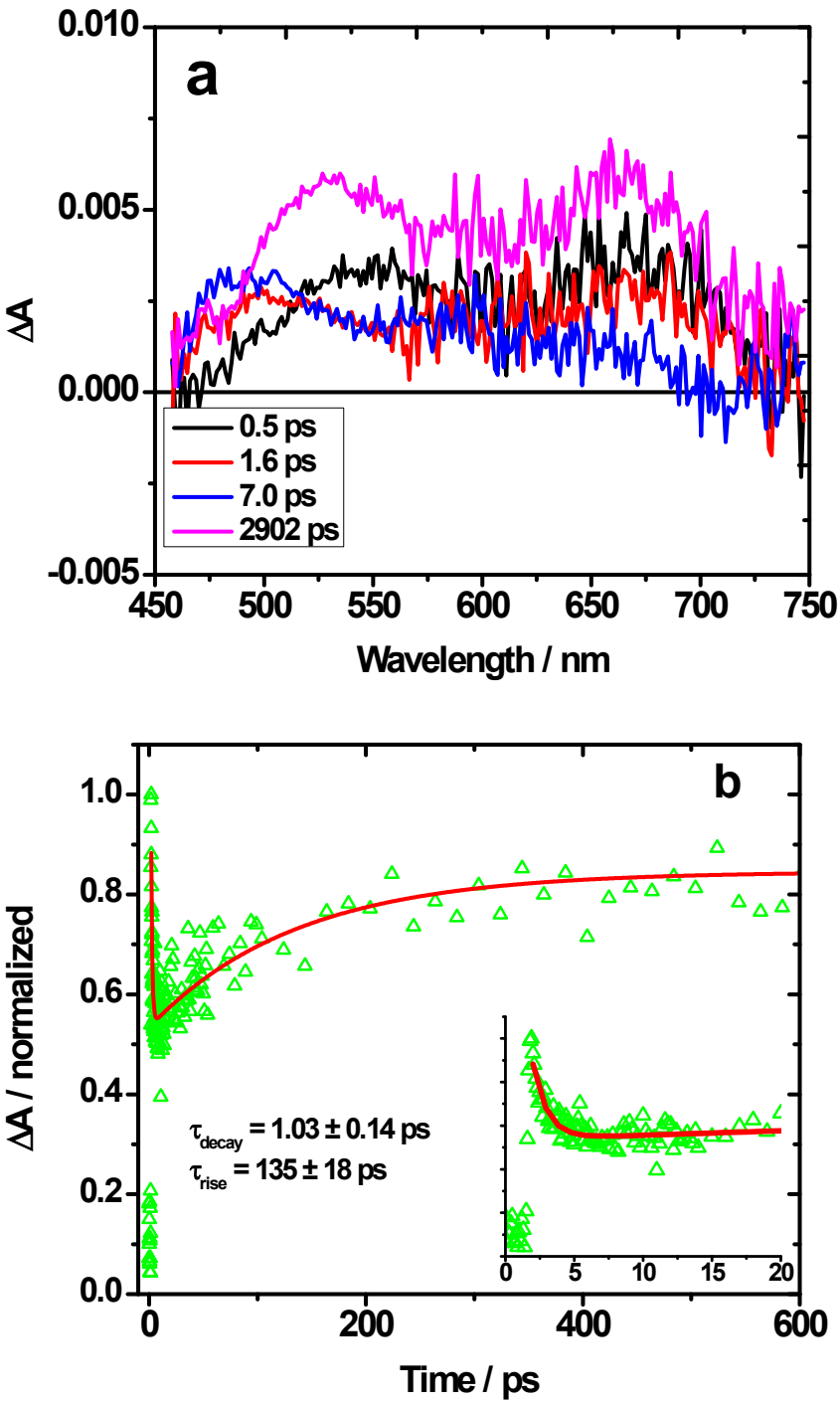

Figure S21. (a) TA spectra of **Ir-2** in CH_2Cl_2 at various delay times (noted in legend). The sample was excited with 390 nm and a power of 0.61 mW. (b) Normalized TA kinetics of **Ir-2** at 671 nm. The inset shows the kinetic fit within the first 20 ps.

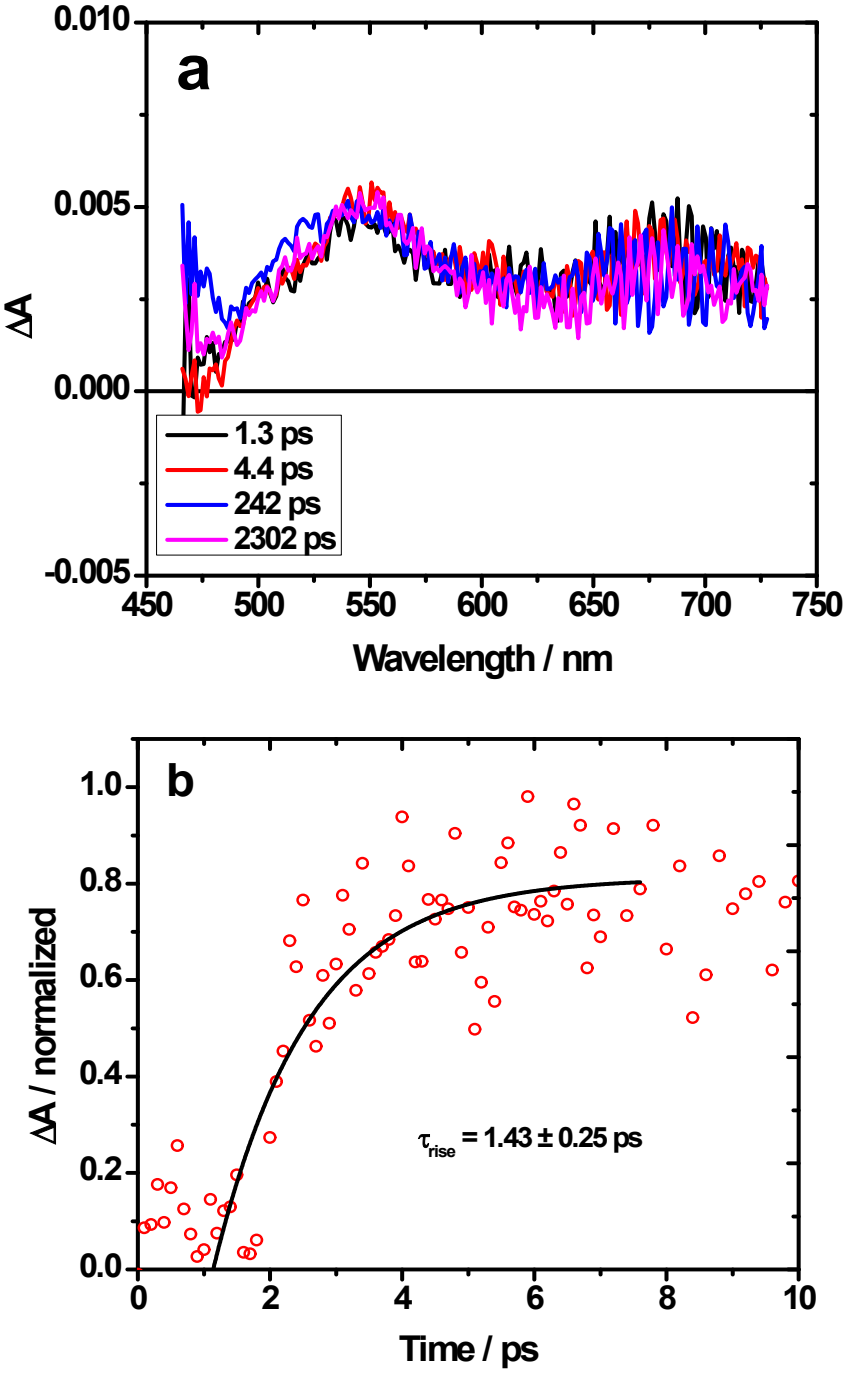

Figure S22. (a) TA spectra of **Ir-3** in CH_2Cl_2 at various delay times (noted in legend). Samples were excited with 390 nm and a power of 0.38 mW. (b) TA kinetics of **Ir-3** in CH_2Cl_2 at 536 nm. There was an initial rise fit with a time constant of 1.43 ± 0.25 ps followed by a long lived component that could not be fit within the first 3 ns.

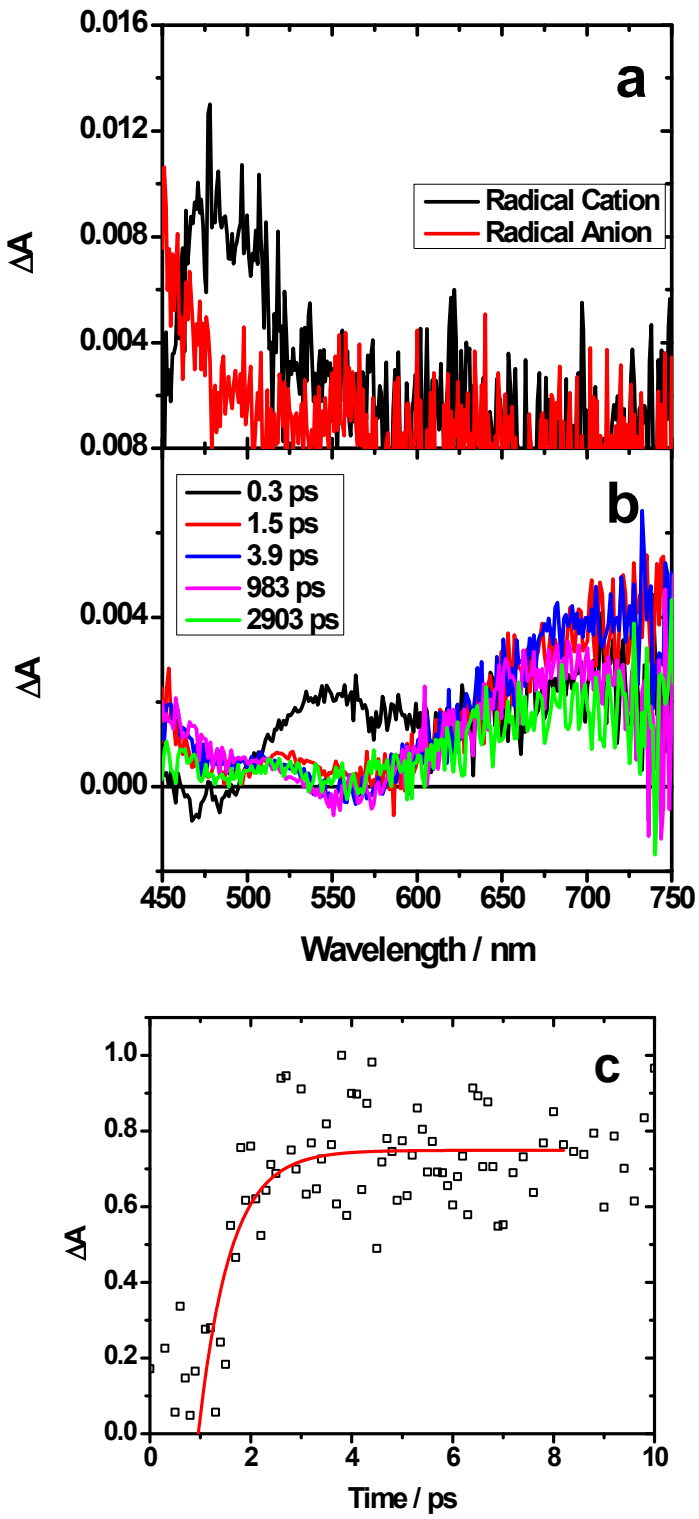

Figure S23. (a) SEC measurements of the ligand **6** in 100 mM TBAP. Anion and cation were generated using a potential of -1400 mV and 1400 mV respectively. (b) TA spectra of the ligand dissolved in CH_2Cl_2 at various delay times (noted in legend). An excitation wavelength of 390 nm and a power of 0.4 mW was used. (c) Kinetic fit of the ligand **6** spectra at 692 nm. There was an initial rise with a lifetime of 0.6 ± 0.3 ps.

Table S2. Natural transition orbitals (NTOs) representing the 3rd excited state of ligand **6.**

Excited state and properties	Hole	Electron
S_3 299 nm $f = 0.0147$	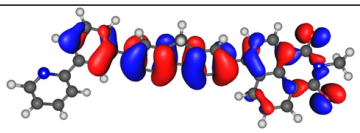 56%	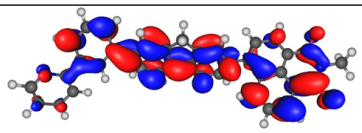 56%
	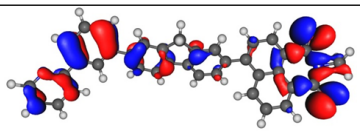 42%	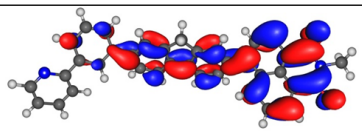 42%

Table S3. Emission quantum yields of **Ir-1 – Ir-3** and ligand **6** in different solvents

	λ_{em}/nm (τ_{em}/μs); Φ_{em}			
	CH_2Cl_2	CH_3CN	Toluene	Acetone
Ir-1[a]	606 (10.8); 0.081	611 (30.1); 0.017	642 (24.1); 0.012	612 (17.6); 0.022
Ir-2[a]	594 (44.5); 0.15	603 (31.7); 0.031	624 (27.5); 0.047	603 (40.0); 0.060
Ir-3[a]	609 (2.23), 640 (2.24); 0.18	627 (1.00); 0.048	596 (0.19), 654 (0.19); 0.029	628 (0.58); 0.054
6[b]	498 (-); 0.60	521 (-); 0.43	450 (-); 0.64	-

[a] Degassed CH_3CN solution of $[Ru(bpy)_3]Cl_2$ (Φ_{em} = 0.042, λ_{ex} = 436 nm) was used as the reference. [b] 1 N sulfuric acid solution of quinine bisulfate (Φ_{em} = 0.546, λ_{ex} = 347.5 nm) was used as the reference

Table S4. Natural transition orbitals contributing to the fluorescence transition from the lowest singlet excited state to the singlet ground state for ligand **6**

Singlet energy	Electron	Hole
473 nm